Journal of Cardiovascular Magnetic Resonance®, 4(2), 233–243 (2002)

VENTRICULAR FUNCTION

Temporal Evolution of Left Ventricular Strain Late After Repair of Coarctation of the Aorta Using 3D MR Tissue Tagging

Alistair A. Young,[1,*] Brett R. Cowan,[2] Christopher J. Occleshaw,[3] Helen C. Oxenham,[2] and Thomas L. Gentles[4]

[1]*Department of Anatomy with Radiology and* [2]*Department of Medicine, University of Auckland, Private Bag 92019, 85 Park Road Grafton, Auckland, New Zealand*
[3]*Cardiac Radiology and* [4]*Paediatric Cardiology, Green Lane Hospital, Auckland, New Zealand*

ABSTRACT

Purpose: Following repair of coarctation of the aorta (CoA), LV mass is increased along with morbidity and mortality. Previous studies have reported increased shortening indices and impaired diastolic function. However, direct measurements of local material motion and temporal evolution of strain have been lacking.

Methods: Magnetic resonance (MR) tissue tagging was used to quantify regional three-dimensional myocardial deformation throughout systole and much of diastole in 14 patients (aged 19–23) who had CoA repair 17–23 years previously, and 15 age-, sex- and BSA-matched normal volunteers (NV).

Results: Mass to end-diastolic volume ratio was increased in the CoA group (1.23 ± 0.12 g/mL CoA vs. 1.14 ± 0.10 g/mL NV, $p = 0.039$*), together with ejection fraction (65.3 ± 4.4 vs. 60.8 ± 1.9%,* $p = 0.001$*) and systolic blood pressure (132.5 ± 14.5 vs. 117.3 ± 11.6 mmHg,* $p = 0.004$*). At end-systole, circumferential shortening was normal, but longitudinal shortening was decreased (14.9 ± 1.3 vs. 16.8 ± 1.4%,* $p < 0.001$*). Although systolic strain rates were not significantly different, early diastolic strain rate (EDSR) in the CoA group was increased in the circumferential direction (−71 ± 23 vs. −52 ± 20%/sec,* $p = 0.029$*), but decreased in the longitudinal direction (−27 ± 12 vs. −39 ± 11%/sec,* $p = 0.015$*). Longitudinal shortening and circumferential EDSR were related to*

*Corresponding author. Fax: (649) 3737484; E-mail: a.young@auckland.ac.nz

right arm–leg pressure gradient ($R^2 = 0.20$, $p = 0.016$ and $R^2 = 0.38$, $p < 0.001$, respectively) and to mass index ($R^2 = 0.18$, $p = 0.024$ and $R^2 = 0.14$, $p = 0.049$, respectively).

Conclusions: MR tagging allows quantitative information on the temporal evolution of myocardial deformation. Directionally dependent changes in strain evolution are seen late after CoA repair. These changes are related to both persistent arm–leg pressure gradient and degree of hypertrophy and may be indicators of developing dysfunction.

Key Words: *Coarctation of the aorta; MR tagging; Ventricular function; Diastolic function; Computer modeling*

INTRODUCTION

Coarctation of the aorta (CoA) is a common congenital cardiovascular malformation which is often repaired in childhood with surgical aortoplasty (1,2). Although short-term outcome is excellent, long-term sequelae include increased rates of hypertension, LV hypertrophy (LVH), coronary artery disease, congestive heart failure, and premature death (1,3). Studies have reported increased LV mass by echocardiography (4–7), and enhanced ejection fraction (EF) and shortening indices by both echocardiography and radionuclide ventriculography (4,6,7). A normal early diastolic filling velocity has been reported by radionuclide ventriculography (6), but E/A ratio is reduced by Doppler echocardiography (4,7). However, these imaging techniques do not allow quantitative measurement of local muscle contraction and relaxation (myocardial strain). Since LVH is known to lead to reduced systolic strains (8,9), it is anticipated that the hypertrophy following CoA repair will lead to systolic strain abnormalities. In addition, diastolic strain-relaxation indices have been found to be impaired in LVH due to aortic stenosis, but normal in athletes with "physiological" hypertrophy (10). The purpose of this study was, therefore, to quantify the regional variation and temporal evolution of three-dimensional (3D) myocardial strain in a series of patients late after repair of CoA, together with matched normal volunteers.

The 3D motions of a large number of specific material points throughout the LV were reconstructed from multislice-tagged magnetic resonance (MR) images with a previously validated finite element modeling method (9,11). Myocardial displacement, rotation, and strain were quantified on a regional basis. Tags were tracked through all frames of the cine sequences, allowing reconstruction of diastolic relaxation, as well as systolic contraction. This provided novel information on the temporal evolution of myocardial deformation in both healthy volunteers and CoA subjects.

METHODS

Study Population

Fifteen patients (age 19–26, four female) with isolated CoA who had undergone surgical repair 17–23 years previously were selected consecutively from a surgical register on the basis of age and suitability for MRI. There was no history of other cardiac disease and no cardio-active medications. The control group consisted of 15 age-, sex- and body surface area (BSA)-matched normal volunteers (NV) who had no history of cardiac disease. All subjects had resting ECG, right arm and leg blood pressure measurements, and standard echocardiographic examination prior to MR imaging. None had evidence of abnormal cardiac function on ECG, blood pressure, echo, or MRI investigations. All studies were approved by institutional review and ethics committees, and all subjects gave informed consent.

Magnetic Resonance Imaging

All imaging was performed on a 1.5 T Siemens Vision magnet with a phased-array body coil. Prospectively gated untagged cardiac cine images were acquired in eight or nine short-axis slices and three long-axis slices using a segmented k-space pulse sequence ($TE/TR = 4.8/9.9$ msec, flip angle = 15°, FOV 280–350 mm, seven or nine views per segment, 128 image matrix) with view-sharing (giving 11–19 frames per slice). Each slice was acquired during a breath hold of 15–19 cardiac cycles at end-tidal lung volume. The short axis slices spanned the heart from apex to base with a slice thickness of 8.0 mm and interslice gap of 0.0–

3.0 mm. The long-axis image slices were acquired at equal 60° increments around the LV central axis, starting at the plane passing through the midseptum, center of the LV cavity, and LV free-wall.

Short-axis tagged images of the heart were acquired at the same positions as the cine images using a prospectively gated, view-shared, segmented k-space version of the SPAMM imaging sequence (12). The tag spacing in the orthogonal grid pattern was 8 mm and the tag lines were oriented at 45° relative to the imaging axes. The imaging parameters were the same as those used for the breath-hold cine MRI acquisition described above, except for TE/TR = 4.0/8.9 msec (giving a temporal resolution of the view-shared reconstructed images of either 35 or 45 msec, depending on heart rate). A set of six long-axis tagged image slices were also acquired at equal 30° increments around the LV central axis. Figure 1 shows typical short-axis tagged images. Good quality image stripes were obtained throughout the cardiac cycle, enabling diastolic, as well as systolic analysis of strain patterns. Note that in all imaging sequences, the last approximately 10% of diastole was not imaged in order to detect the R-wave trigger.

Reconstruction of 3D Shape and Deformation

End-diastolic volume (EDV), end-systolic volume (ESV) and myocardial wall volume were determined interactively from the untagged images using guide-point modeling (13). Volumes were calculated from the model using numerical integration. LV mass was calculated from the average of the myocardial volumes at ED and ES, multiplied by the specific gravity 1.05 g/mL. The distance between the apex and center of the base was measured in each of the three long-axis untagged image slices and averaged to provide an independent estimate of base–apex longitudinal shortening.

Tag stripes were semiautomatically tracked in each image, resulting in a grid of tracked stripe points with a spacing of approximately 2 mm between points. The 3D displacements of all tag points were reconstructed with the aid of a finite element model, as described previously (9,11). Myocardial strain measures at any point in the model were calculated using standard methods of continuum mechanics (11,14). The percentage shortening or lengthening of myocardium was calculated as the change in length as a percentage of the end-diastolic length in each of the circumferential (C), longitudinal (L) and radial (R) directions:

$$\%S_{\mathrm{A}} = \frac{\mathrm{d}l_{\mathrm{ED}} - \mathrm{d}l_T}{\mathrm{d}l_{\mathrm{ED}}} 100\% \quad (1)$$

where A is one of the C, L, or R directions, $\%S_{\mathrm{A}}$ is the percentage shortening or lengthening at time T in this direction, $\mathrm{d}l_{\mathrm{ED}}$ and $\mathrm{d}l_T$ are the lengths of an infinitesimal material line segment (oriented in this direction at ED) at ED and T, respectively. Note that lengthening is negative and shortening positive in this description. Shear strains (α_{AB}) were calculated as the change in angle between infinitesimal line segments initially oriented at right angles in the A and B directions, where A and B are any of the C, L, or R directions (not both the same) (14). Rotational displacement and LV twist about the LV central axis were calculated as the change in angle about an axis joining the centroids of the base and apex at each time (11).

For the purposes of temporal strain evolution, end-systole (ES) was taken to be the time of least model

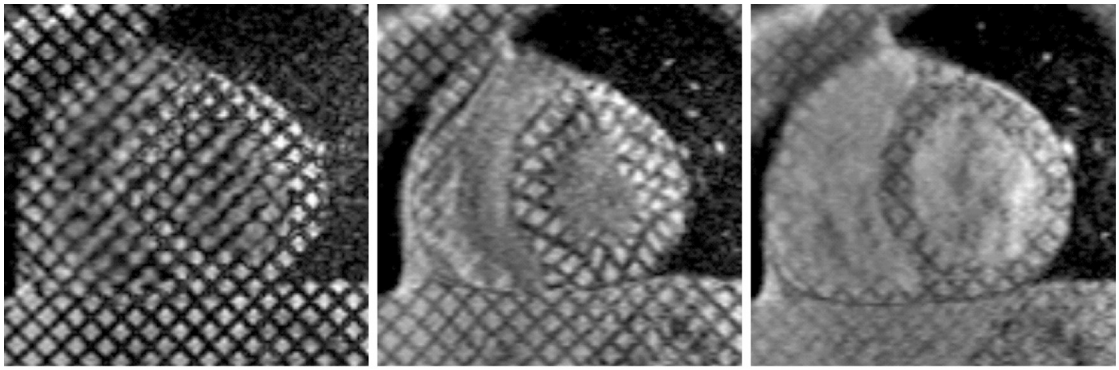

Figure 1. Short-axis tagged MR images at the midventricular level for a typical CoA subject showing good tag persistence throughout the cardiac cycle (a) end-diastole, (b) end-systole, (c) late diastole.

cavity volume in the tagged model reconstructions. Strain rates were calculated for each individual subject as the slope of the straight line of best fit to the strain/time relationship over specified time intervals. For systole, the interval was from frame 2 (i.e., ED + 1) to frame ES − 1. For early diastole, the interval was from ES to frame ES + 3.

Statistical Analysis

Displacement and strain data were averaged into 16 regions in accordance with the recommendations of the American Society of Echocardiography Committee on Standards (15). The LV was divided into three longitudinal levels (apex, mid and base), which, in turn, were divided into four (for the apex) or six (for midventricle and base) circumferential regions. Repeated measures ANOVA was used to test for regional differences in displacement and strain within each group, with two-way ANOVA to test for differences between groups. Global volume, hemodynamic data and strain rates were compared with an unpaired *t*-test. A *p* value of less than 0.05 was required to reject the null hypothesis that there were no differences between groups or regions.

RESULTS

Hemodynamics and Global Function

Of the 15 CoA patients studied, one had insufficient tagged images for 3D quantification, leaving 29 cases in which 3D strain could be quantified (14 CoA and 15 NV). Hemodynamic data and functional parameters measured from the untagged MR images are shown in Table 1 for these subjects. Systolic blood pressure (SBP), EF, and mass/EDV ratio were significantly greater in the CoA group. The gradient between right arm and leg SBP was increased (range − 14 to 38, median 12 mmHg in the CoA group). The length between apex and base shortened less in the CoA group ($p < 0.001$). Mass indexed to BSA tended to be higher in the CoA group, but this did not achieve significance ($p = 0.07$). Overall, these data indicate an increased EF, hypertension, and mild hypertrophy in the CoA group.

Myocardial Displacement and Strain

In all cases, tag stripes could be tracked through all frames of the acquisition. The root mean squared error between tracked image stripe points and reconstructed 3D model tag points (0.86 ± 0.34 mm) was comparable to the image pixel size (1.1–1.5 mm). The time taken as ES (the time of least tagged model cavity volume) was not significantly different (355 ± 28 msec CoA vs. 349 ± 20 msec NV, $p =$ NS), indicating no difference in ejection time between groups. This time corresponded to maximum global circumferential and longitudinal shortening (Figs. 2 and 3) and occurred approximately two frames prior to the first frame in which the mitral valve could be seen to be open. The two frames after ES, therefore, approximately correspond with the normal 70–90 msec isovolumic relaxation period.

Table 1

Hemodynamic Data and Global Function Derived from Untagged MR Images

	CoA ($n = 14$)	NV ($n = 15$)	*p* value
BSA (m^2)	1.86 ± 0.24	1.83 ± 0.25	NS
SBP (mmHg)	132.5 ± 14.5	117.3 ± 11.6	0.004
RALG (mmHg)	11.9 ± 13.2	− 13.1 ± 8.9	<0.001
EDV (mL)	147.4 ± 36.3	141.0 ± 26.8	NS
ESV (mL)	51.4 ± 15.7	55.2 ± 10.5	NS
SV (mL)	96.0 ± 23.0	85.8 ± 17.0	NS
EF (%)	65.3 ± 4.4	60.8 ± 1.9	0.001
Mass (g)	179.6 ± 41.9	161.2 ± 35.2	NS
Mass:BSA (g/m^2)	95.6 ± 14.2	87.2 ± 10.1	NS (0.07)
Mass:EDV (g/mL)	1.23 ± 0.12	1.14 ± 0.10	0.039
Base-Apex L (%)	14.2 ± 2.3	17.4 ± 2.3	<0.001

BSA: Body Surface Area; SBP: Right Arm Systolic Blood Pressure; RALG: Right Arm–Leg Blood Pressure Gradient; EDV: End-Diastolic Volume; ESV: End-Systolic Volume; SV: Stroke Volume; EF: Ejection Fraction; Base-Apex L: Base-Apex Length Change from ED to ES.

Circumferential shortening strain ($\%S_C$) showed no significant differences between CoA and NV groups at ES (20.2 ± 1.2 vs. 20.1 ± 1.2%, p = NS) (Fig. 2). Systolic strain rate was similar (84 ± 8%/sec CoA vs. 84 ± 6%/sec NV, p = NS), whereas early diastolic relaxation was faster in the CoA group (−71 ± 23%/sec CoA vs. −52 ± 20%/sec NV, $p = 0.029$) (Fig. 2a). The normal regional variation in $\%S_C$ at ES was preserved in the CoA group, with very similar values between groups across all regions (Fig. 2b).

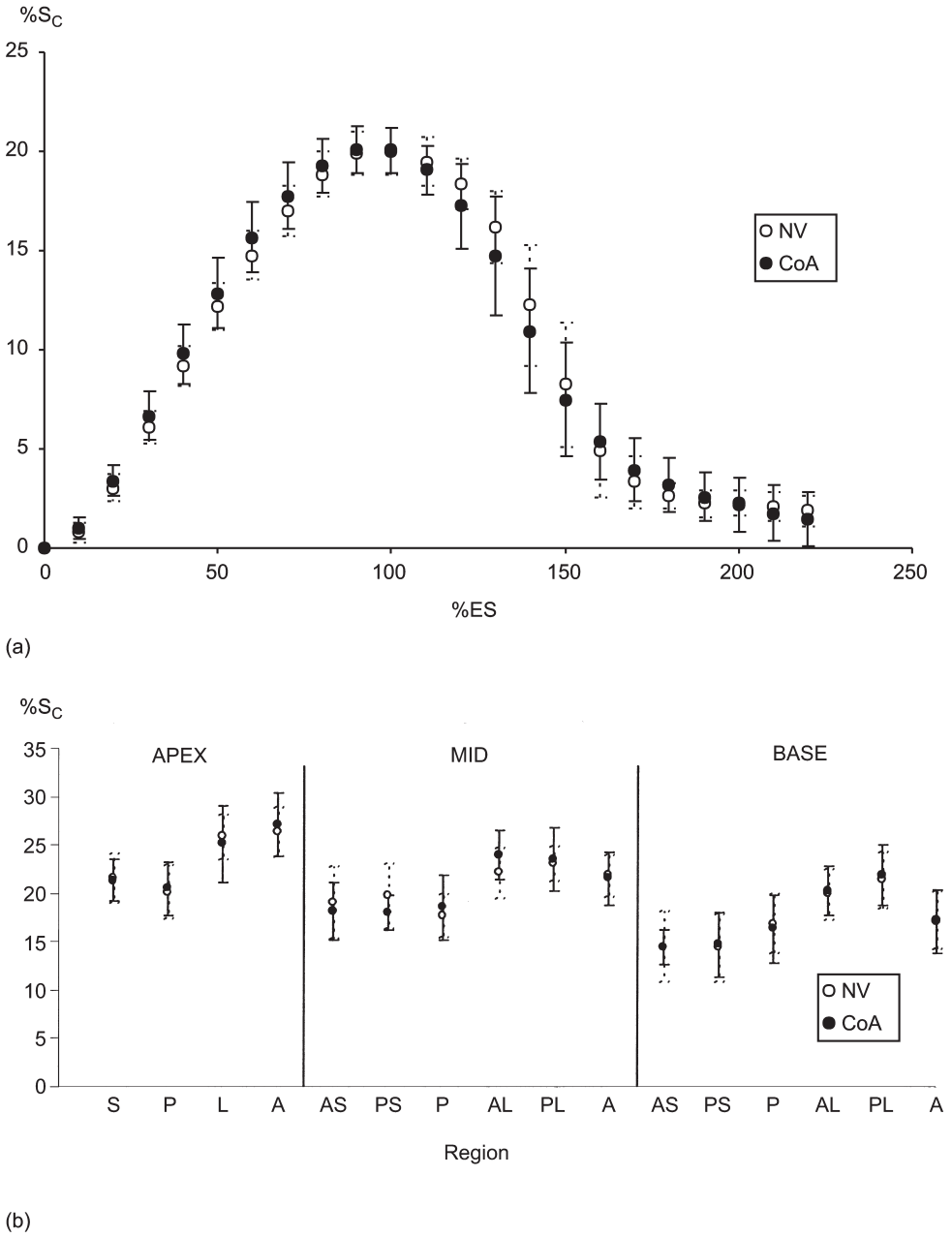

Figure 2. Circumferential shortening strain $\%S_C$. Error bars denote SD (NV dashed). (a) Average $\%S_C$ as a function of time (time indexed as a percentage of ES). Values were linearly interpolated at 10% intervals between the nearest two frames of the cine sequence. (b) Regional $\%S_C$ at ES. A: anterior, P: posterior, L: lateral S: septum.

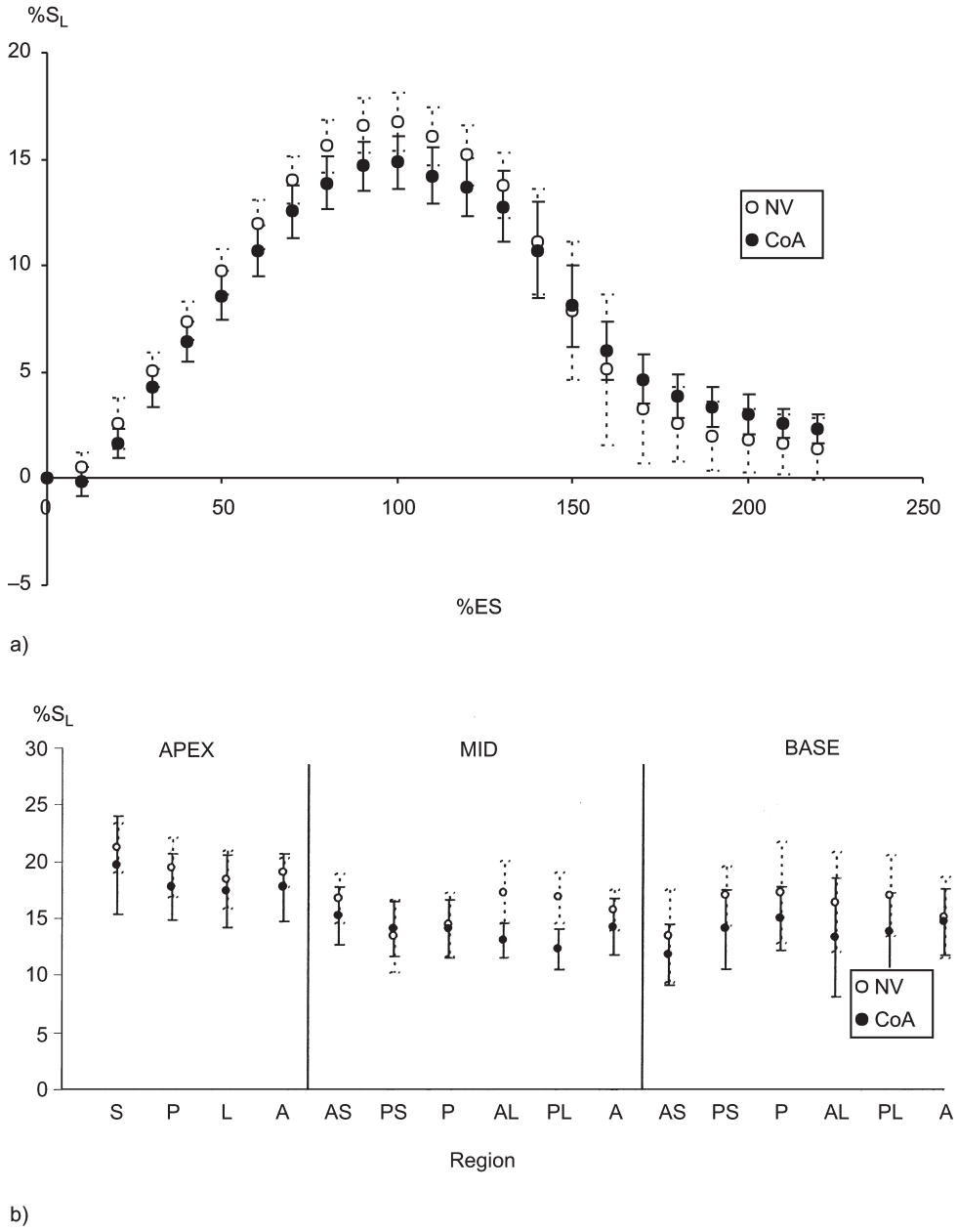

Figure 3. Longitudinal shortening strain $\%S_L$. (a) Average $\%S_L$ as a function of time; (b) regional $\%S_L$ at ES. Symbols as for Fig. 2.

Longitudinal shortening strain ($\%S_L$) showed a small but significant decrease in the CoA group at ES ($14.9 \pm 1.3\%$ CoA vs. $16.8 \pm 1.4\%$ NV, $p < 0.001$) (Fig. 3). This decrease was consistent across groups in most regions (Fig. 3b). Systolic longitudinal strain rate tended to be reduced but did not reach significance ($65 \pm 7\%$/sec CoA vs. $70 \pm 5\%$/sec NV, $p = 0.06$). Early diastolic relaxation of longitudinal strain was reduced in the CoA group ($-27 \pm 12\%$/sec CoA vs. $-39 \pm 11\%$/sec NV, $p = 0.015$). Longitudinal shortening is related to the descent of the base plane towards the apex during systole and ascent away from the apex during diastole. At ES, there was less absolute displacement of the basal regions (11.4 ± 1.3 mm CoA

vs. 12.5 ± 1.1 mm NV, $p = 0.022$) and less relative displacement between apex and base regions in the CoA group (8.7 ± 1.0 mm vs. 10.0 ± 0.9 mm, $p = 0.001$).

The shear strain associated with LV torsion (α_{CL}) was greater in the CoA group at ES (5.82 ± 0.81 vs. 4.95 ± 1.09°, $p = 0.022$). However, early diastolic strain-relaxation rate of α_{CL} was normal (−27 ± 10°/sec CoA vs. −25 ± 11°/sec NV, $p =$ NS). Ventricular torsion is related to LV twist (apical rotation about the LV central axis relative to the rotation of the base). LV twist at ES tended to be higher than normal but this did not reach significance (13.9 ± 2.0° CoA vs. 12.3 ± 2.6° NV, $p = 0.09$) (Fig. 4). LV twist increased at approximately constant rate through systole (56 ± 10°/sec CoA vs. 53 ± 12°/sec NV, $p =$ NS), followed by a slightly faster untwisting in early diastole (−76 ± 15°/sec CoA vs. −66 ± 19°/sec NV, $p =$ NS).

The transverse shear angle α_{CR} is associated with transmural gradient of LV torsion (9) and was more negative at ES at the base in the CoA group (−6.39 ± 1.67° vs. −5.09 ± 1.57°, $p = 0.041$), indicating increased torsion on the endocardial wall relative to the epicardial wall in this region. The transverse shear strain α_{LR} is associated with transmural differences in longitudinal displacement (9) and was similar between groups. The principal strain associated with maximum shortening at each point (minimum eigenvalue of the strain tensor) was very similar between groups at ES (26.7 ± 1.3 vs. 26.7 ± 1.2%, $p =$ NS).

Resting right arm–leg pressure gradient can be used as a measure of persistent flow abnormalities and residual stenosis in patients with CoA repair (4). Both $\%S_L$ and early circumferential strain-relaxation rate correlated with resting arm–leg pressure gradient ($R^2 = 0.20$, $p = 0.016$ and $R^2 = 0.38$, $p < 0.001$, respectively, see Fig. 5). Significant correlations were also found between $\%S_L$ and mass/BSA index ($R^2 = 0.18$, $p = 0.024$) and between early circumferential strain-relaxation rate and mass/BSA index ($R^2 = 0.14$, $p = 0.049$).

DISCUSSION

MR tagging has previously been used to quantify systolic strain patterns in LVH and hypertension (8,9). Other imaging techniques have shown abnormal diastolic function in LVH (16–18); however, these methods do not allow measurement of material deformation in the heart wall. Recently, MR tagging has also been used to quantify diastolic strain patterns (10,19–21). We have examined systolic and diastolic strain evolution late after CoA repair, in which increased LV mass and hypertension are thought to lead to long-

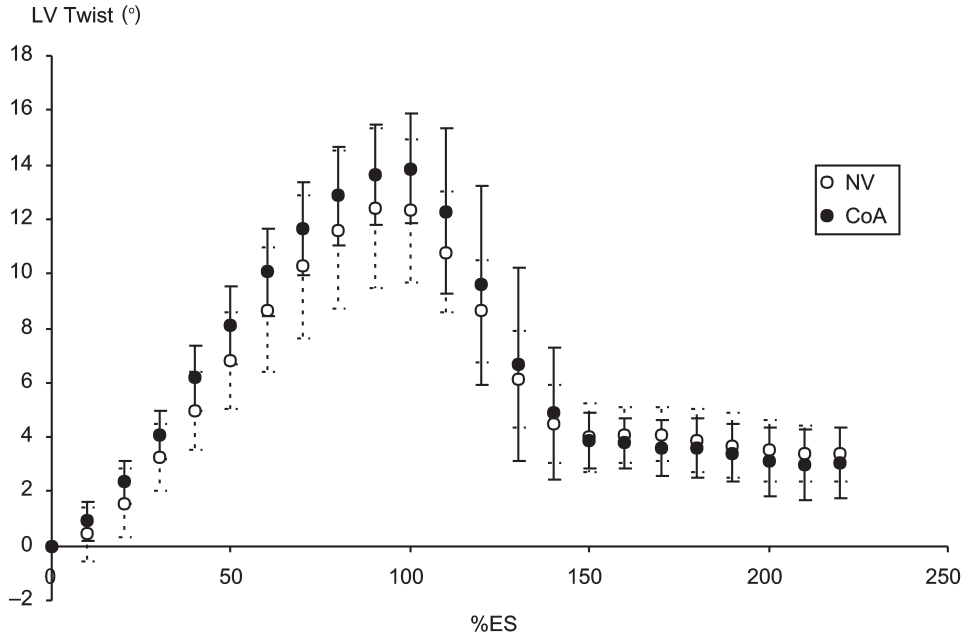

Figure 4. Average LV twist vs. time.

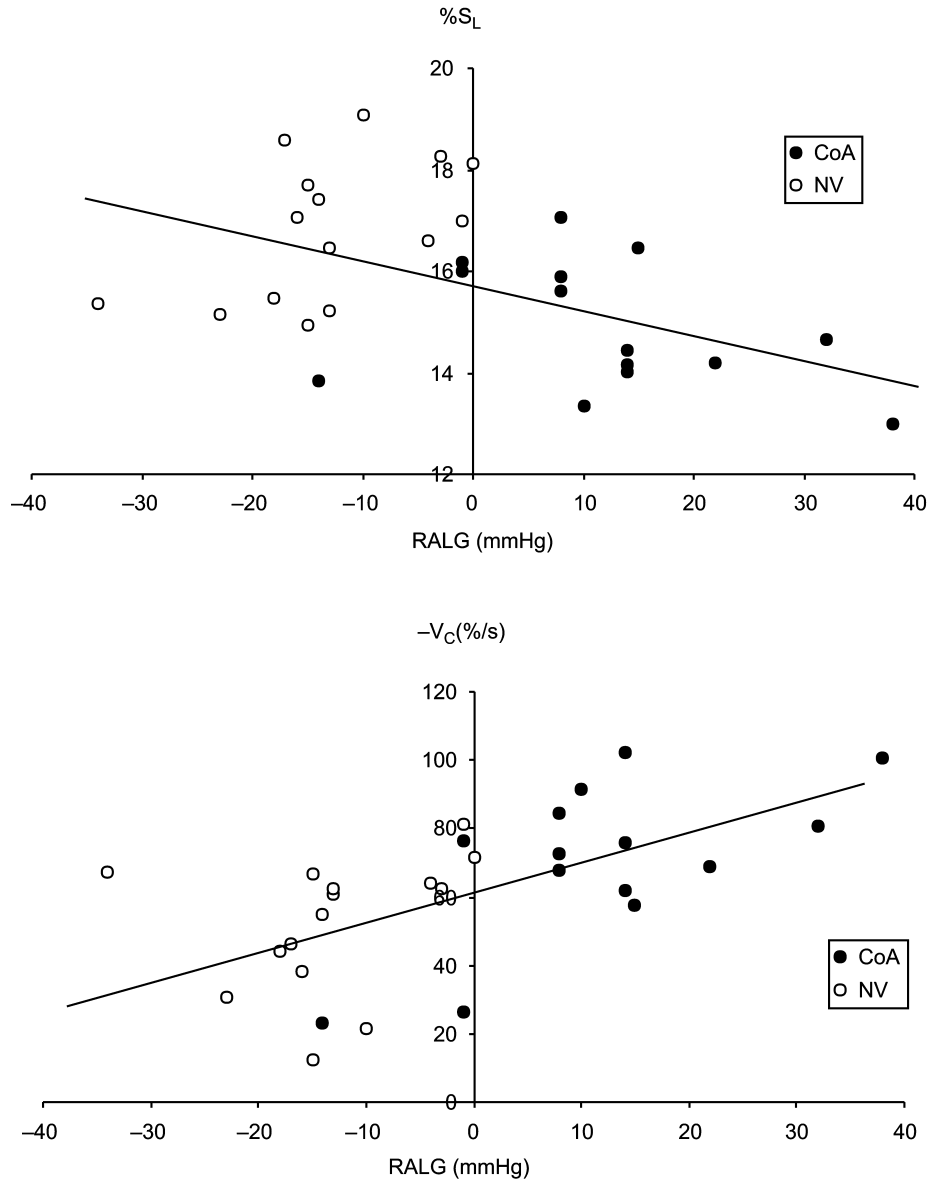

Figure 5. (a) Longitudinal shortening at ES ($\%S_L$) vs. right arm–leg pressure gradient (RALG), with line of best fit. (b) Rate of circumferential strain relaxation in early diastole ($-V_C$) vs. right arm–leg pressure gradient (RALG), with line of best fit. Note lengthening is negative as in Eq. (1).

term cardiac problems. During systole, the CoA group exhibited normal circumferential shortening, reduced longitudinal shortening, and increased LV torsional shear. Early diastolic relaxation of circumferential strain was greater in the CoA group, while relaxation of longitudinal strain was reduced. Both normal and CoA findings are discussed in relation to previous studies below.

Normal Temporal Evolution of Strain

Kuijer (19) recently reported diastolic function in 10 normal volunteers using a 3D MR tagging analysis. Systolic strains were similar to the present study ($\%S_C$ 21 ± 2%, $\%S_L$ 16 ± 2%). Diastolic relaxation of strain was also similar to that observed here, with 50% of $\%S_C$

and $\%S_L$ recovered by 180 msec after ES (corresponding to approx. 150% ES in Figs. 2a and 3a). Diastolic parameters showed a marked age dependence, highlighting the need for age-matched controls.

Stuber et al. (10) quantified diastolic rotation and torsion in 12 patients with aortic stenosis (pressure overload hypertrophy), 11 healthy volunteers, and 11 world class athletes (physiological hypertrophy), using a slice-following short-axis tagging protocol. The temporal evolution of rotation and twist in the controls and athletes were similar to those observed in the present study; however, the magnitude of the ES rotation and torsion was less (apical rotation of $7 \pm 2°$, LV twist of $6 \pm 1°$ at ES for controls) than found here. This difference may reflect differences in the regions calculated (2D slices vs. 3D model regions) or imaging protocols (coached breathing vs. breath-hold). Nagel et al. (21) also quantified diastolic untwisting in 18 patients with chronic anterolateral infarction and 13 normal volunteers, with similar control values for systolic rotation ($12.5 \pm 3.5°$) and early diastolic velocity of untwist ($-67.7 \pm 16.5°$/sec) to the present study. Fogel et al. (22) studied diastolic function in 11 normal infants (age 2–11 months) using a 2D strain analysis on three short-axis tagged slices. Tags were applied at ES and strains were reported at the end of diastole relative to the ES tags; however, the temporal evolution of deformation was not examined.

In contrast to LV twist and rotation, circumferential and longitudinal shortening do not show a rapid recovery phase in early diastole (19). Comparing the velocity in systole with the velocity in early diastole in the current study, LV twist ($53 \pm 12°$/sec systolic vs. $-66 \pm 19°$/sec diastolic) shows a relatively fast recovery, whereas $\%S_C$ ($84 \pm 6\%$/sec systolic vs. $-52 \pm 20\%$/sec diastolic) and $\%S_L$ ($70 \pm 5\%$/sec systolic vs. $-39 \pm 11\%$/sec diastolic) show relatively slow recovery in the early stages of diastole.

Myocardial Kinematics Late After CoA Repair

Long-term sequelae after CoA repair include increased EF, LVH, and hypertension (1–3), each of which were observed in the present study. The degree of residual stenosis has been correlated with LV mass index and SBP percentiles (23,24). Increased velocity of circumferential fiber shortening and increased wall stress to rate-corrected velocity of shortening index have also been observed, suggesting increased contractility (7,25); however, systolic strain rates by tagged MRI were normal in our subjects. Previous analyses of the temporal characteristics of ejection and filling have yielded varying results. Kimball et al. (26) found prolonged systole (contrary to the present study) and time to peak ejection rate using radionuclide ventriculography, with no difference in diastolic variables. Moskowitz (4) found decreased early filling and increased late filling (i.e., greater reliance on the atrial contraction component of filling). The ratio of peak early filling velocity to peak atrial component of the transmitral inflow (*E*/*A* ratio) was reduced (as in Ref. (7)) in relation to LV mass, but *m*-mode normalized peak lengthening velocity was not different. In contrast, Tantengco et al. (27) found increased peak lengthening rates by *m*-mode echo, with normal Doppler mitral inflow parameters. Krogman et al. (5) used biplane angiography with simultaneous pressure catheter measurements at rest and after nitroprusside infusion. LV relaxation and myocardial stiffness were normal, but there was an upward shift of the diastolic pressure–volume curve, which was reversed by nitroprusside. Our results indicate that diastolic material strain indices are directionally dependent, with reduced early relaxation of longitudinal function but augmented early circumferential relaxation. Temporal indices of longitudinal function may be sensitive indicators of systolic and diastolic dysfunction (28,29). Future long-term followup studies may shed light on the development of these parameters with disease progression and their relation to chamber function.

Mechanisms for Temporal Abnormalities in Strain

This study found increased EF but normal $\%S_C$ and reduced $\%S_L$. The increased EF may be a geometric effect due the mild hypertrophy in the CoA group, since incompressible models predict an increase in EF with increasing hypertrophy (30). The cause of the decrease in $\%S_L$ is unknown but may also be related to the degree of hypertrophy, since $\%S_L$ correlated with mass–BSA index. One possible mechanism may be an increased afterload on longitudinal fibers due to the compression of an increased myocardial mass (circumferential shortening may not be as affected due to trabeculation on the inner LV wall).

The resting arm–leg pressure gradient can be used as an index of persistent flow abnormalities and residual stenosis, which may be a mechanism for increased impedance to LV ejection and increased LV mass (4). The fact that both $\%S_L$ and early circumferential strain-relaxation rate correlated with resting arm–leg pressure

gradient indicates that LV strain evolution is affected by chronic flow abnormalities, perhaps via the associated LVH. However, the high degree of separation between the two groups of values of arm–leg pressure gradient may have lead to an artificial correlation, as no correlations were seen in the individual groups (except for the CoA group in the case of early circumferential strain-relaxation rate, Fig. 5b, $p = 0.011$). Further study is needed to resolve this issue.

Limitations

This study did not attempt to alter loading conditions or image during exercise. Many diastolic parameters have been shown to be load dependent (31). However, the similar ejection time and EDV between the two groups indicates that preload was comparable. In this study temporal resolution was limited to 35–45 msec and the instants of aortic valve closure and mitral valve opening could not be precisely determined. Advances in fast imaging techniques will allow higher temporal resolution and more reliable estimates of strain velocity in the future (20).

ACKNOWLEDGMENTS

This work was supported by the Auckland Medical Research Foundation and an equipment grant from the Wellcome Trust (UK).

REFERENCES

1. Cohen, M.; Fuster, V.; Steele, P.M.; Driscoll, D.; McGoon, D.C. Coarctation of the Aorta: Long-Term Follow-Up and Prediction of Outcome After Surgical Correction. Circulation **1989**, *80*, 840–845.
2. Johnson, M.C.; Canter, C.E.; Straws, A.W.; Spray, T.L. Repair of Coarctation of the Aorta in Infancy: Comparison of Surgery and Balloon Angioplasty. Am. Heart J. **1993**, *25*, 454–458.
3. Maron, B.J.; O'Neal, H.J.; Rowe, R.D.; Mellitis, E.D. Prognosis of Surgically Corrected Coarctation of the Aorta: A 20-year Post-Operative Appraisal. Circulation **1973**, *47*, 119–126.
4. Moskowitz, W.B.; Sckieken, R.M.; Mosteller, M.; Bossano, R. Altered Systolic and Diastolic Function in Children After "Successful" Repair of Coarctation of the Aorta. Am. Heart J. **1990**, *120*, 103–109.
5. Krogman, O.N.; Rammos, S.; Jakob, M.; Corin, W.J.; Hess, O.M.; Bourgeois, M. Left Ventricular Diastolic Late After Coarctation Repair in Childhood: Influence of Left Ventricular Hypertrophy. J. Am. Coll. Cardiol. **1993**, *21*, 1454–1460.
6. Carpenter, M.A.; Dammann, J.F.; Watson, D.D.; Jedeikin, R.; Tomkins, D.G.; Beller, G.A. Left Ventricular Hyperkinesia at Rest and During Exercise in Normotensive Patients 2 to 27 years After Coarctation Repair. J. Am. Coll. Cardiol. **1985**, *6*, 879–886.
7. Leandro, J.; Smallhorn, J.F.; Benson, L.; Musewe, N.; Balfe, J.W.; Dyck, J.D.; West, L.; Freedom, R. Ambulatory Blood Pressure Monitoring and Left Ventricular Mass and Function After Successful Surgical Repair of Coarctation of the Aorta. J. Am. Coll. Cardiol. **1992**, *20*, 197–204.
8. Palmon, L.C.; Reichek, N.; Yeon, S.B.; Lima, J.; Hoffman, E.; Axel, L. Intramural Myocardial Shortening in Hypertensive Left Ventricular Hypertrophy with Normal Pump Function. Circulation **1994**, *89*, 122–131.
9. Young, A.A.; Kramer, C.M.; Ferrari, V.A.; Axel, L.; Reichek, N. Three-Dimensional Left Ventricular Deformation in Hypertrophic Cardiomyopathy. Circulation **1994**, *90*, 854–867.
10. Stuber, M.; Scheidegger, M.B.; Fischer, S.E.; Nagel, E.; Stienemann, F.; Hess, O.M.; Boesiger, P. Alterations in the Local Myocardial Motion Pattern in Patients Suffering from Pressure Overload Due to Aortic Stenosis. Circulation **1999**, *100*, 361–368.
11. Young, A.A.; Kraitchman, D.L.; Dougherty, L.; Axel, L. Tracking and Finite Element Analysis of Stripe Deformation in Magnetic Resonance Tagging. IEEE Trans. Med. Imaging **1995**, *14*, 413–421.
12. Axel, L.; Dougherty, L. Heart Wall Motion: Improved Method of Spatial Modulation of Magnetization for MR Imaging. Radiology **1989**, *172*, 349–350.
13. Young, A.A.; Cowan, B.R.; Thrupp, S.F.; Hedley, W.J.; Dell'Italia, L.J. Left Ventricular Mass and Volume: Fast Calculation with Guide-Point Modeling on MR Images. Radiology **2000**, *216*, 597–602.
14. Fung, Y.C. *Foundations of Solid Mechanics*; Prentice-Hall, Inc.: Englewood Cliffs, NJ, 1965.
15. Schiller, N.B.; Shah, P.M.; Crawford, M.; DeMaria, A.; Devereux, R.; Feigenbaum, H.; Gutgesell, H.; Reichek, N.; Sahn, D.; Schnittger, I.; Silverman, N.H.; Tajik, J. Recommendations for Quantification of the Left Ventricle by Two-Dimensional Echocardiography. J. Am. Soc. Echo **1989**, *2*, 358–367.
16. Lorell, B.H.; Grossman, W. Cardiac Hypertrophy: The Consequences for Diastole. J. Am. Coll. Cardiol. **1987**, *9*, 1189–1193.
17. Shapiro, L.M.; Gibson, D.G. Patterns of Diastolic Dysfunction in Left Ventricular Hypertrophy. Br. Heart J. **1988**, *59*, 438–445.
18. Spirito, P.; Maron, B.; Bonow, R.O. Noninvasive Assessment of Left Ventricular Diastolic Function: Comparative Analysis of Doppler Echocardiographic

and Radionuclide Angiographic Techniques. J. Am. Coll. Cardiol. **1986**, *7*, 518–526.
19. Kuijer, J.P.A. Myocardial Deformation Measured with Magnetic Resonance Tagging. Ph.D. Thesis, Free University, Amsterdam, 88–104.
20. Scott, C.H.; Ivey, B.S.; Duffy, K.J.; Ferrari, V.A.; Ivandjiiski, D.; Axel, L.; St. John Sutton, M.G. Complex Left Ventricular Angular Motion and Torsion Can Be Quantified Using High Frame Rate Tagged Cardiac Magnetic Resonance Imaging. J. Cardiovasc. Magn. Reson. **1999**, *1* (4), 322, (Abstract).
21. Nagel, E.; Stuber, M.; Lakatos, M.; Scheidegger, M.B.; Boesiger, P.; Hess, O.M. Cardiac Rotation and Relaxation After Anterolateral Myocardial Infarction. Coron. Artery Dis. **2000**, *11*, 261–267.
22. Fogel, M.A.; Weinberg, P.M.; Hubbard, A.; Haselgrove, J. Diastolic Biomechanics in Normal Infants Utilizing MRI Tissue Tagging. Circulation **2000**, *102*, 218–224.
23. Ong, C.M.; Canter, C.E.; Gutierrez, F.R.; Sekarski, D.R.; Goldring, D.R. Increased Stiffness and Persistent Narrowing of the Aorta After Successful Repair of Coarctation of the Aorta: Relationship to Left Ventricular Mass and Blood Pressure at Rest and with Exercise. Am. Heart J. **1992**, *123*, 1594–1600.
24. Johnson, M.C.; Gutierrez, F.R.; Sekarski, D.R.; Ong, C.M.; Canter, C.E. Comparison of Ventricular Mass and Function in Early Versus Late Repair of Coarctation of the Aorta. Am. J. Cardiol. **1994**, *73*, 698–701.
25. Kimball, T.R.; Reynolds, J.M.; Mays, W.A.; Khoury, P.; Claytor, R.P.; Daniels, S.R. Persistent Hyperdynamic Cardiovascular State at Rest and During Exercise After Successful Repair of Coarctation of the Aorta. J. Am. Coll. Cardiol. **1994**, *24*, 194–200.
26. Kimball, B.P.; Shurvell, B.L.; Houle, S.; Fulop, J.C.; Rakowski, H.; McLaughlin, P.R. Persistent Ventricular Adaptations in Postoperative Coarctation of the Aorta. J. Am. Coll. Cardiol. **1986**, *8*, 172–178.
27. Tantengco, M.V.; Ross, R.D.; Humes, R.A.; Sullivan, N.M.; Joshi, V.M.; Clapp, S.K.; Epstein, M.L. Enhanced Resting Left Ventricular Filling in Patients with Successful Coarctation Repair and Exercise-Induced Hypertension. Am. Heart J. **1997**, *134*, 1082–1088.
28. Henein, M.Y.; Gibson, D.G. Long Axis Function in Disease. Heart **1999**, *81*, 229–231.
29. Oki, T.; Tabata, T.; Yamada, H.; Wakatsuki, T.; Shinohara, H.; Nishikado, A.; Iuchi, A.; Fukuda, N.; Ito, S. Clinical Application of Pulsed Doppler Tissue Imaging for Assessing Abnormal Left Ventricular Relaxation. Am. J. Cardiol. **1997**, *79*, 921–928.
30. Dumesnil, J.G.; Souchri, R.M. Effect of Geometry of the Left Ventricle on the Calculation of Ejection Fraction. Circulation **1982**, *65*, 91–98.
31. Mandinov, L.; Eberli, F.R.; Seiler, C.; Hess, O.M. Diastolic Heart Failure. Cardiovasc. Res. **2000**, *45*, 813–825.

Received June 11, 2001
Accepted October 29, 2001